DOI: 10.1002/
Article type: Full Paper

Fabricating a Homogeneously Alloyed AuAg Shell on Au Nanorods to Achieve Strong, Stable, and Tunable Surface Plasmon Resonances

*Jianfeng Huang,Yihan Zhu, Changxu Liu, Yunfeng Zhao, Zhaohui Liu, Mohamed Nejib Hedhili, Andrea Fratalocchi and Yu Han**

J. Huang, Dr. Y. Zhu, Dr. Y. Zhao, Z. Liu, Prof. Y. Han
Advanced Membranes and Porous Materials Center, Physical Sciences and Engineering Division, King Abdullah University of Science and Technology (KAUST), Thuwal, 23955-6900, Kingdom of Saudi Arabia
E-mail: yu.han@kaust.edu.sa
C. Liu, Prof. A. Fratalocchi
PRIMALIGHT, Electrical Engineering, Applied Mathematics and Computational Science, King Abdullah University of Science and Technology (KAUST), Thuwal, 23955-6900, Kingdom of Saudi Arabia
Dr. M. N. Hedhili
Imaging and Characterization Core Lab, King Abdullah University of Science and Technology (KAUST), Thuwal, 23955-6900, Kingdom of Saudi Arabia

Keywords: Au nanorods, Ag stability, homogeneous AuAg alloys, tunable surface plasmon resonances, high plasmonic activities

Colloidal metal nanocrystals with strong, stable, and tunable localized surface plasmon resonances (SPRs) could be useful in a corrosive environment for many applications including field-enhanced spectroscopies, plasmon-mediated catalysis, *etc*. Here, a new synthetic strategy is reported that enables the epitaxial growth of a homogeneously alloyed AuAg shell on Au nanorod seeds, circumventing the phase segregation of Au and Ag encountered in conventional synthesis. The resulting core-shell structured bimetallic nanorods (AuNR@AuAg) have well-mixed Au and Ag atoms in their shell without discernible domains. This degree of mixing allows AuNR@AuAg to combine the high stability of Au with the superior plasmonic activity of Ag, thus outperforming seemingly similar nanostructures with monometallic shells (*e.g.*, Ag-coated Au NRs (AuNR@Ag) and Au-coated Au NRs (AuNR@Au)). AuNR@AuAg is comparable to AuNR@Ag in plasmonic activity, but that it is markedly more stable towards oxidative treatment. Specifically, AuNR@AuAg and

AuNR@Ag exhibit similarly strong signals in surface-enhanced Raman spectroscopy (SERS) that are some 30-fold higher than that of AuNR@Au. When incubated with a H_2O_2 solution (0.5 M), the plasmonic activity of AuNR@Ag immediately and severely decayed, whereas AuNR@AuAg retained its activity intact. Moreover, the longitudinal SPR frequency of AuNR@AuAg can be tuned throughout the red wavelengths (~620-690 nm) by controlling the thickness of the AuAg alloy shell. Our synthetic strategy is versatile to fabricate AuAg alloyed shells on different shaped Au, with prospects for new possibilities in the synthesis and application of plasmonic nanocrystals.

1. Introduction

Metal nanocrystals have rich and fascinating optical properties that arise from the excitation of localized surface plasmon resonances (SPRs).[1] Among the numerous plasmonic nanocrystals of different sizes, shapes, and compositions, anisotropic Au nanorods (AuNRs) are of particular interest because the wavelength and strength of their longitudinal SPRs (LSPRs) can be adjusted by tuning the aspect ratio of the rods.[2] As illustrated by the finite-difference time-domain (FDTD) simulation, with the aspect ratio of a AuNR increasing from 1 (*i.e.*, isotropic sphere) to 4.4, the maximum intensity of the electric field rendered by LSPRs is enhanced by ~125 times, while the resonance wavelength undergoes a considerable bathochromic shift from 530 to 850 nm (**Figure S1**). The intense LSPRs of AuNRs in the near-infrared (NIR, > 780 nm) region are particularly useful for biological applications;[3] however, a wide range of applications requires plasmonic responses in the visible range of the spectra.[4] For example, Wang *et al.*[4a] and MiKi *et al.*[4b] reported the SPR induced efficient visible light harvesting for enhancing the visible photocatalytic activities of ceria and titania, respectively. Smolyaninov *et al.*[4c]demonstrated a magnifying superlens whose design was based on the optics of surface plasmon polaritons in the visible frequency range. Tricarico *et al.*[4d] investigated the plasmonic layered structures for conformal electromagnetic cloaking

covers at visible wavelengths. Therefore, positioning strong LSPR of rod-shaped nanocrystals at wavelengths of < 700 nm is desirable.

According to Gans' equation that was initially developed to deal with ellipsoids,[5] the LSPR frequency (ω) of rod-shaped nanocrystals can be approximately determined by:

$$\varepsilon'(\omega) = -\frac{(1-P)}{P}\varepsilon_m\,, \qquad (1)$$

where ε'(ω) is the real part of the metal's dielectric function, ε_m is the medium's dielectric function, and P is the depolarization factor for the longitudinal axis of the rod-shaped particle; the strength and width of the resonance is characterized by a quality factor (Q):[6]

$$Q = \frac{\omega\,(d\varepsilon'/d\omega)}{2\,[\varepsilon''(\omega)]^2}, \qquad (2)$$

where ε" (ω) is the imaginary part of the metal's dielectric function. Thanks to the smaller dielectric function (both the real and imaginary part) of elemental Ag compared with elemental Au, Ag nanorods (AgNRs) have an even stronger LSPR (**Equation 2**) at a shorter wavelength (**Equation 1**) than do AuNRs of the same aspect ratio (see **Figure S1**). Because direct synthesis is difficult, pre-synthesized AuNRs are commonly coated with a Ag shell as a strategy to prepare AgNRs, allowing control of the aspect ratio of AgNRs and thus their LSPRs.[7] Although AgNRs have intriguing plasmonic properties, they have not been widely used in practical applications, mainly because their susceptibility to oxidation makes them unstable, severely deteriorating its intrinsic high plasmonic activity.

Several attempts have been made to improve the stability of Ag-based plasmonic nanocrystals. For example, an extra protective SiO_2 layer was deposited on Ag nanostructures;[8] however, thick and dense SiO_2 limited the approach of target molecules to the surface of Ag, while thin and porous SiO_2 provided insufficient protection.[9] Efforts to deposit a protective Au layer caused partial dissolution of Ag as a result of a replacement reaction between Ag crystals and Au precursors.[10] Recently, a report investigating a

replacement reaction-free coating of Au on Ag found that the thickness of Au must be delicately controlled to avoid diminishing the plasmonic activity of the inner Ag core.[11] An alternative and perhaps more effective method is to *homogeneously alloy* elemental Ag with elemental Au in nanocrystals. The role of Au to stabilize Ag through alloying has been documented in the literature:[12] a higher oxidation potential was required to trigger the replacement reaction of Ag when it was alloyed with Au;[12a] the replacement reaction of Ag was hindered when the molar ratio of Au/Ag was greater than 0.17.[12b] A number of diverse approaches have been developed to prepare AuAg alloyed nanocrystals including laser ablation,[13] sputter deposition,[14] phase-transfer,[15] replacement reaction,[16] digestive ripening,[17] interface diffusion,[18] and co-reduction of Au and Ag precursors.[19] However, these efforts have paid little attention to achieving compositional homogeneity in the crystals produced because they did not consider the chemical stability of Ag. Two recent studies indicated that uniform mixing of Au and Ag atoms (compositional homogeneity) in the nanocrystal is required to achieve the "stabilizing" effect and that Ag remains susceptible to oxidation if the two elements are segregated into large domains (results were verified in this work (*vide infra*)).[20] These two studies are currently the only successful examples of the preservation of both plasmonic activity and chemical stability by synthesizing homogeneously alloyed AuAg nanocrystals; however, their synthetic methods were limited to the production of isotropic (nearly spherical) nanocrystals. In one of these studies,[20a] the combined use of NH_4OH and $NaBH_4$ facilitated a uniform mixing of Au and Ag during co-reduction, but the strong reducing power of $NaBH_4$ and the consequential fast reduction kinetics resulted in the formation of small round crystals (< 10 nm) with a poor size distribution. In the other study, Yin's group fabricated fully alloyed AuAg nanospheres with good compositional homogeneity through the high temperature (~1000 °C) annealing of SiO_2-coated Au-Ag core-shell nanopolyhedrons.[20b] This method requires complex procedures (*e.g.*, coating and removal of SiO_2) and harsh annealing conditions, but more importantly, it cannot produce

alloyed nanocrystals with special shapes (*e.g.*, rods, cubes) other than spheres because regardless of their original shape, at such high annealing temperatures, nanocrystals will fuse into spherical particles (see **Figure S2**). Therefore, shape-dependent SPR properties are yet unavailable for homogeneously alloyed nanocrystals synthesized by the existing methods, and their SPRs are confined within the characteristic wavelengths of the Au and Ag spheres (*i.e.*, ~380-520 nm).[21]

In this paper, we endeavoured to fabricate homogeneously alloyed AuAg shells on AuNRs with the aim of integrating the merits of the AuAg alloy (high plasmonic activity and excellent stability) with the advantages of anisotropic nanorods (strong and adjustable LSPRs). To this end, we developed a facile synthetic strategy with no constraints on nanocrystal shape. This strategy took advantage of a *simultaneous* and *slow* addition of Au and Ag precursors into pre-synthesized AuNR solutions containing a strong reducing agent, which guarantees compositional homogeneity of Au and Ag atoms across the newly formed shells. The resulting bimetallic nanorods (designated as AuNR@AuAg) manifested superior chemical stability and strong LSPRs, as unraveled by our oxidation tests and SERS measurements. Additionally, the LSPR frequency of AuNR@AuAg could be delicately tuned across the red wavelength range (620-690 nm) by controlling the thickness of the alloy shell, enriching the available SPR wavelengths imparted by stable AuAg alloy nanocrystals.

2. Results and Discussion

A typical synthetic procedure is illustrated in **Figure 1a**: $AgNO_3$ (100 μL, 3 mM) and $HAuCl_4$ (100 μL, 2 mM) were infused into a AuNR seed solution (0.5 mL) containing cetyltrimethylammonium chloride (CTAC) and sodium ascorbate at a pumping rate controlled by a programmable syringe pump with dual syringes. The single-crystalline AuNRs synthesized following our previous procedures were 55.0 ± 4.7 nm long and 12.6 ± 0.8 nm

wide (**Figure 1b**).[22] Assuming the added Au and Ag precursors are completely reduced to form bimetallic shells on the AuNRs, the Au/Ag molar ratio was 3/2 in the shell.

In the first experiment, Au and Ag precursors were rapidly added to the seed solution at a pumping rate of 6 mL/min (equivalent to a one-shot injection of the full 100 μL of precursors in 1 second, **Figure 1a**). We observed that the AuNR seeds grew into thicker nanorods with pointy ends, and that the original AuNRs and the later-grown shells were discernible by transmission electron microscopy (TEM) (**Figure 1c**). Previously, a similar co-reduction method (a one-shot injection of a strong reducing agent into AuNR solutions containing a mixture of $HAuCl_4$ and $AgNO_3$) was used to fabricate shells on AuNRs; the shells were considered to be homogeneous alloys of Au and Ag.[23] However, this may have been a mistaken presumption because the pronounced difference in redox potentials of $HAuCl_4$ and $AgNO_3$ likely results in the sequential reduction of Au and Ag and consequently phase separation.[24] To address this question, we employed high-angle annular dark-field scanning transmission electron microscopy (HAADF-STEM), which is sensitive to the atomic number (Z) of the specimen and can therefore distinguish Au from Ag if there are phase segregations, to probe the as-synthesized nanorods. The HAADF-STEM images (**Figure 2a and b**) clearly revealed that the shell was inhomogeneous in composition, containing discrete Au islands (brighter contrast), which were attached to the AuNR seeds and buried in a continuous outer layer of Ag (lower contrast). Energy dispersive X-ray (EDX) spectroscopy line-scan analysis confirmed the compositional inhomogeneity in the shells with a Au-enriched inside and a pure-Ag outside (**Figure 2c)**. These results demonstrate that the preferential reduction of Au over Ag indeed leads to phase segregation in the newly grown shells, and that the outermost surfaces of the obtained nanorods (hereafter designated as AuNR@Au@Ag) are composed of Ag and not a AuAg alloy.

We aimed to overcome this phase segregation by adding the precursors to the seed solution slowly over time instead of by the one-shot (or fast addition) method. We predicted

that by slowly adding the precursors, only a tiny amount of fresh Au and Ag precursors would be available at any time point during the seeded-growth, forcing Au and Ag to gradually deposit in a well-mixed fashion. On the basis of this hypothesis, we synthesized another batch of material by following the aforementioned procedure, but we decreased the pumping rate to 0.005 mL/min (**Figure 1a**). As illustrated in **Figure 1d**, the obtained material was similar in morphology to that synthesized by the fast addition protocol (*i.e.*, AuNR@Au@Ag), consisting of thick nanorods with pointy ends. However, the contrast between AuNR seeds and the outer AuAg shell in the TEM image became less distinguishable in the rod-body areas, suggesting that the composition distribution in the shell might be different in the two materials. Electron diffraction (ED) demonstrated that each individual nanorod remained a single crystal, and the HRTEM image accordingly showed a perfect epitaxial growth of the shell from the AuNR (**Figure 1e**). As expected, these nanorods had a uniform Z-contrast throughout the entire later-grown shell in the HAADF-STEM images (**Figure 2d and e**), suggesting that Au and Ag atoms were uniformly mixed in the shell. This conclusion was supported by the analysis of the EDX line-scan (**Figure 2f**), where Au and Ag signals occurred concomitantly during electron beam scanning across the nanorod. EDX elemental maps acquired over one small half of a nanorod showed a uniform overlap in Au and Ag distributions, further confirming the fully alloyed nature of the shell (**Figure 2g-i**). These nanorods are hereafter designated as AuNR@AuAg, which feature homogeneously alloyed AuAg shells (compositional homogeneity) and epitaxially deposited on AuNRs (structural homogeneity), and they are expected to render strong and stable LSPRs.

To investigate the LSPR properties of the AuNR@AuAg, the UV-vis-NIR extinction spectra of its aqueous suspension were collected and compared with those of AuNR@Au@Ag, AuNR@Au, and AuNR@Ag. Here, AuNR@Au and AuNR@Ag denoted the structures that were synthesized by adding only $HAuCl_4$ or $AgNO_3$, respectively, with all other conditions identical to those employed for AuNR@AuAg (see **SI** for synthetic details).

AuNR@Au and AuNR@Ag are nanocrystals with peanut and cuboid shapes, respectively (see **Figure S3**). The original AuNRs that seeded the growth of the four core/shell structures exhibited a broad LSPR peak at 850 nm, with a full-width at half-maximum (FWHM) of ~178 nm (**Figure 3a**). In agreement with previous work, the AuNR@Au manifested a similarly broad LSPR peak (FWHM: ~ 150 nm) that was slightly blue-shifted (peaking at 794 nm) due to the decreased aspect ratio and largely intensified owing to enhanced absorption and scattering.[25] Compared with AuNR@Au, both AuNR@Ag and AuNR@Au@Ag with pure Ag shells enclosing the AuNR exhibited sharper (FWHM: ~100 nm and ~103 nm, respectively) and markedly more blue-shifted LSPR bands (peak at 669 nm and 658 nm, respectively) (**Figure 3b and c**), demonstrating the advantageous optical properties of Ag (as discussed earlier). Likewise, the AuNR@AuAg also possessed a sharper (FWHM: ~125 nm) and more blue-shifted LSPR (peak at 676 nm) in comparison to AuNR@Au (**Figure 3d**). The large blue-shift in LSPR observed for AuNR@Au@Ag and AuNR@AuAg relative to the original AuNR seed was the result of the combined effect of crystal size, shape and composition (see **Figure S4 and S5** for detailed analysis). These results indicate that homogeneously incorporated Ag in the AuAg shell can effectively improve the plasmonic activities of Au.

The chemical stabilities of the four materials against a strong oxidizing environment (*i.e.*, H_2O_2 in this work) were characterized by monitoring changes in their LSPRs when they were transferred from H_2O to H_2O_2 (0.5 M). Because AuNR@Au is made of pure Au, it showed a strong resistance to H_2O_2 etching, as evidenced by the nil reduction in its extinction intensity (**Figure 3a)**. The preservation of plasmonic property was also reflected by the identical color of AuNR@Au suspended in H_2O and H_2O_2 (**inset of Figure 3a**); Accordingly, TEM showed the intact particle shape of AuNR@Au after treatment with H_2O_2 (**Figure S6a**). AuNR@Ag and AuNR@Au@Ag, which are characterized by strong and sharp LSPRs associated with their Ag shell, suffered an immediate degradation (within 5 s) upon exposure to H_2O_2 (0.5 M),

as indicated by the vivid color changes of their suspensions from greenish in H_2O to dark brown in H_2O_2. Accordingly, in the UV-vis-NIR spectra, the characteristic LSPR band was severely deteriorated and concomitantly a weak and broad band extending to longer wavelengths arose (**Figure 3b and c**). TEM showed that after treatment with H_2O_2, AuNR@Ag and AuNR@Au@Ag NRs were severely deformed and aggregated as a consequence of Ag etching (**Figure S6b and c**), which likely accounted for the observed broad extinction.[26] The etching effect of H_2O_2 on Ag was also verified by X-ray photoelectron spectroscopy (XPS), which showed the appearance of the Ag oxide, the oxidizing product of Ag, in treated AuNR@Ag and AuNR@Au@Ag samples (**Figure S7**). In striking contrast, the intense plasmonic activity of AuNR@AuAg was fully inert to the etching effect of H_2O_2. As displayed in **Figure 3d**, after substituting H_2O_2 for H_2O, the LSPR peak was only slightly red-shifted due to the larger dielectric constant of H_2O_2 than that of H_2O,[27] while the peak intensity remained the same even after 1 h incubation. The extinction spectra agreed well with the suspension colors using H_2O and H_2O_2 as solvents (**inset of Figure 3d**). The stability of AuNR@AuAg was further corroborated by the TEM images showing perfect shape preservation (**Figure S6d**), and the XPS measurements revealing the identical chemical state for Ag before and after treatment with H_2O_2 (**Figure S7**). In addition, we observed a negative shift of 0.10 eV in the Ag $3d_{5/2}$ binding energy of AuNR@AuAg relative to that of pure Ag-shelled AuNR@Ag or AuNR@Au@Ag (see XPS profiles in **Figure S8**). This result is consistent with previous findings, suggesting that Ag redistributes its *s*-charge to the *d*-channel upon alloying with Au.[28] Since Ag tends to use its *s*-electron to get involved in the oxidization chemistry,[29] the depleted electron density in the *4s*-subshell of Ag as a consequence of the charge redistribution[28] accounts for the effective resistance of AuNR@AuAg to oxidation by H_2O_2. To ensure compatibility with long-term applications, stability was further tested in a series of higher H_2O_2 concentrations for prolonged incubation times of up to 24 h (**Figure 3e and f**). We found that even with harsher treatments, the LSPR

peak intensity was well maintained at 98~99% of the original value within experimental errors, except for a continuous red-shift observed with the gradual increase in H_2O_2 concentration (**Figure 3f**). The red-shift is jointly induced by the larger dielectric constant of H_2O_2 than that of H_2O and light oxidization of Ag component (see **Figure S9**). We also tested the stability of AuNR@AuAg in ammonia solution. In the presence of oxygen, ammonia can effectively etch elemental Ag through oxidative complexing to form soluble $[Ag(NH_3)_2]^+$ complex in the solution.[30] We found that after being incubated in ammonia solution (0.5 M) for 1h, the AuNR@AuAg maintained its LSPR band intensity at ~97% of the original value (**Figure S10**). In contrast, AuNR@Au@Ag lost the band intensity by ~41% after the same treatment (**Figure S10**). There was no remarkable decay within an additional 1h, due to the shortage of oxygen supply. These results further confirm that AuNR@AuAg is superior to AuNR@Au@Ag in stability. Overall, these results demonstrated that AuNR@AuAg NRs have similarly strong LSPR as that of Ag-coated AuNRs, whereas they are considerably more stable against oxidative etching.

We found that the LSPR frequency of AuNR@AuAg NRs can be finely tailored within the red wavelengths by simply varying the total amount of the added Au and Ag precursors (with an unchanged Au/Ag ratio of 3/2) for the seeded growth. Specifically, when the volume of the precursors increased from 80 to 150 μL, the extinction band experienced a linear blue-shift from ca. 690 to ca. 620 nm (**Figure 4**). The monotonous shift with the addition of more precursors was attributed partially to the slightly decreased aspect ratios of the NRs as the shells grew thicker (**Figure S11**) and partially to the increased Ag atomic fraction in the material (including both the AuNR core and the AuAg shell) from 29.0% to 42.5%, as determined by inductively coupled plasma-atomic emission spectroscopy (**Figure 4b**). Meanwhile, the bandwidth of the LSPR was slightly reduced from ~135 to ~120 nm. Regardless of shell thickness, AuNR@AuAg samples have markedly narrower LSPR bands than do those of the starting AuNR (~178 nm) or AuNR@Au (~151 nm), implying a sharper

resonance associated with elemental Ag. The intense, sharp, stable, and tunable LSPR of AuNR@AuAg appears promising for a multitude of optical applications.

In a proof-of-concept experiment, we demonstrated the merits of AuNR@AuAg by comparing its colloidal SERS activity with those of AuNR@Au@Ag, AuNR@Au, and AuNR@Ag in both H_2O and H_2O_2. We used 4-Nitrobenzenethiol (4-NBT) as the Raman probe, and the excitation wavelength for each material was chosen based on their LSPR determined from the extinction spectra (see Experimental Section for SERS measurement details). The strongest 4-NBT SERS band, located at 1334 cm^{-1},[22] was used as a benchmark for comparing the performance of the four substrates. When the particles were dispersed in H_2O for measurements, the three Ag-containing substrates (*i.e.,* AuNR@AuAg, AuNR@Au@Ag, and AuNR@Ag) manifested comparable SERS signals of 30-fold, 31-fold, and 42-fold, respectively, stronger than that of the pure Au substrate (*i.e.,* AuNR@Au) (**Figure 5a**), confirming the superior activity of Ag nanostructures over their Au counterparts in field-enhanced spectroscopies. Upon the addition of H_2O_2 to the suspensions, AuNR@Au@Ag and AuNR@Ag, with pure Ag in the outmost shell exposed to H_2O_2 oxidation, substantially lost their intense SERS activities; in contrast, AuNR@AuAg and AuNR@Au efficiently retained their SERS signals, indicating that the alloyed shells of AuNR@AuAg could be as robust as pure Au in resisting etching by H_2O_2 (**Figure 5b**). Overall, these results confirmed that AuNR@AuAg integrates the high plasmonic activity of Ag with the excellent chemical stability of Au, acting as an ideal SERS substrate in terms of both sensitivity and durability for molecular detection.

There are a few additional points we wish to highlight regarding the method used here. **(*i*)** The sufficiently small amount of precursor that was infused into the seed solution and reduced instantaneously at each time point was paramount to the compositional homogeneity in the shell of AuNR@AuAg. The amount of infused precursor was determined by the infusion rate (*e.g.*, 0.005 mL/min in this work) multiplied by the concentration (*e.g.*, 3 mM for

$AgNO_3$ and 2 mM for $HAucl_4$ in this work). To maximize the compositional homogeneity, one would expect the rate to be as small as possible; a rate of 0.005 mL/min was at an extreme low in the rate range, below which (*e.g.,* 0.0025 mL/min) a capillary lift of the seed solution into the syringes will take place. Alternatively, one could decrease the concentration of the precursors; however this will prolong the reaction time. The concentrations of the precursors used here were a good compromise between the compositional homogeneity and reaction time. **(*ii*)** The stability and sharpness of the LSPR of AuNR@AuAg were strongly dependent on the concentration ratio of $AgNO_3$ to $HAuCl_4$ during synthesis ($AgNO_3/HAuCl_4$ = 3/2 in the synthesis in this work). High Ag content would favor plasmonic activity but reduce stability. Two extreme examples are the structures synthesized using $AgNO_3/HAuCl_4$ = 5/0 and 0/5. As discussed earlier, the resulting structures AuNR@Ag and AuNR@Au were less stable and had weaker plasmonic activity, respectively (**Figure 5**). At a ratio of $AgNO_3/HAuCl_4$ = 3/2, AuNR@AuAg efficiently combines the merits of Au and Ag with no detriment to either plasmonic activity or stability. **(*iii*)** The use of a moderately strong reducing agent (*i.e.,* ascorbate sodium) is also crucial for the fabrication of AuNR@AuAg. With an even stronger reducing agent like $NaBH_4$, homogeneous nucleation and growth of AuAg particles in the solution would be favored over the epitaxial seeded growth of the AuAg alloyed shell on AuNRs (**Figure S12**). When a medium reducing agent (*e.g.,* ascorbic acid) was used, Au was preferentially deposited at the rod ends, while Ag was enriched outside the shell, coating the rod bodies. Like the other pure Ag-coated structures, this structure was unstable even in a low concentration of H_2O_2 (0.5 M) (**Figure S13**). **(*iv*)** Our method is facile and versatile, and it can be easily adapted to coat homogeneously alloyed AuAg shells on Au nanoscrystals of different shapes. As an example, Au polyhedron@AuAg is presented in **Figure S14**.

3. Conclusion

In conclusion, a facile yet effective and versatile seeded growth strategy has been developed that enables the epitaxial deposition of homogeneously alloyed AuAg shells on pre-synthesized AuNRs. The resulting AuNR@AuAg exhibits stronger LSPRs and higher SERS activity than do pure Au nanostructures with comparable sizes and shapes (*e.g.*, AuNR and AuNR@Au), made possible by the incorporation of Ag. On the other hand, in comparison to other AuAg bimetallic core-shell structures with pure Ag shells (*e.g.*, AuNR@Au@Ag and AuNR@Ag), AuNR@AuAg possesses similarly high plasmonic activity but significantly improved stability against oxidation by H_2O_2, benefiting from the alloyed nature of the shell. Our study reveals that the fabrication of AuAg alloyed shells by co-reduction of Au and Ag precursors is not as straightforward as presumed in previous studies. The sufficiently slow addition of the precursors along with a suitable reducing agent is the key to success, without which Au and Ag atoms are easily segregated in the shell as a consequence of sequential rather than simultaneous reduction. By simply adjusting the amount of $HAuCl_4$ and $AgNO_3$, we were able to exquisitely tune the LSPR frequency of the AuNR@AuAg within the red region of the spectrum (620–690 nm). Given the strong, stable, and tunable LSPR properties, the AuNR@AuAg nanorods promise many plasmonic applications because of their high performance and long lifetime, especially in an oxidizing environment. Our synthetic strategy holds the potential to be extended to the preparation of core@alloyed shell materials with other crystal shapes (*e.g.*, cube, polyhedrons) and elements (*e.g.*, Pd, Pt).

4. Experimental Section

Synthesis of AuNR@AuAg, AuNR@Au, AuNR@Ag, and AuNR@Au@Ag: Starting AuNRs were synthesized and cleaned following the procedure introduced in our previous work,[22] with the exception that the growth process was limited to 9.5 h. To prepare the AuNR@AuAg nanorods, $AgNO_3$ (100 μL, 3 mM) and $HAuCl_4$ (100 μL, 2 mM) that were pre-sucked in separate syringes were infused at 0.005 mL/min into a AuNR seed solution (0.55 mL, ~0.92

nM) containing a capping agent, CTAC (73 mM), and a strong reducing agent, sodium ascorbate (9.1 mM). After 20 min all the precursors had been ejected, and the product was washed and collected *via* centrifuge at 7800 rpm for 8 min. To synthesize AuNR@Au, AuNR@Ag, and AuNR@Au@Ag, the same procedure for the synthesis of AuNR@AuAg was followed, with the exception that for AuNR@Au and AuNR@Ag, $HAuCl_4$ (250 μL, 2 mM) and $AgNO_3$ (166.7 μL, 3 mM) were added, respectively. Here, the volume of $HAuCl_4$ (*i.e.,* 250 μL) and $AgNO_3$ (*i.e.,* 166.7 μL) were determined to ensure an equal number of stoichiometric metal atoms in the shells of AuNR@Au, AuNR@Ag, and AuNR@AuAg. For AuNR@Au@Ag, the infusion rate was changed to 6 mL/min.

Characterizations. Extinction spectra were taken on a Varian Cary 5000 UV-vis-NIR spectrophotometer. Low-magnification TEM images were taken on a FEI-Tecnai T12 microscope operated at 120 kV. HAADF-STEM images, EDX line-scan and elemental mappings were acquired on a FEI-Titan ST electron microscope operated at 300 kV. XPS data were collected on an Axis Ultra instrument (Kratos Analytical) with a monochromatic Al K_α X-ray source operating at 150 W under ultrahigh vacuum ($<10^{-8}$ torr) conditions.

SERS measurements. AuNR@Au, AuNR@Ag, AuNR@Au@Ag, and AuNR@AuAg (100 μL, ~0.46 nM) were each incubated with a 4-NTP ethanol solution (5 μL, 0.01 mM) overnight. SERS spectra were recorded on a Horiba Jobin Yvon LabRAM HR-800 spectrophotometer coupled to an Olympus confocal microscope (BX41) with a ×50 objective (NA = 0.50) in the backscattering configuration. The laser excitations were chosen based on the substrates' extinction spectra (Figure 3). Specifically, 660 nm was employed for the three Ag-containing NRs (*i.e.,* AuNR@Ag, AuNR@Au@Ag, and AuNR@AuAg) and 785 nm for the pure Au NRs (*i.e.,* AuNR@Au). The spectra were collected from the suspension using an exposition time of 5 s for all samples in conjunction with a grating of 600 lines/mm.

Supporting Information

Supporting Information is available from the Wiley Online Library or from the author.

Acknowledgements

This research was supported by the KAUST Office of Competitive Research Funds (OCRF) under Awards No. FCC/1/1972-03-01.

Received: ((will be filled in by the editorial staff))
Revised: ((will be filled in by the editorial staff))
Published online: ((will be filled in by the editorial staff))

References

[1] L. M. Liz-Marzan, C. J. Murphy, J. Wang, *Chem. Soc. Rev.* **2014**, *43*, 3820.

[2] a) H. Chen, L. Shao, Q. Li, J. Wang, *Chem. Soc. Rev.* **2013**, *42*, 2679; b) X. Ye, Y. Gao, J. Chen, D. C. Reifsnyder, C. Zheng, C. B. Murray, *Nano Lett.* **2013**, *13*, 2163.

[3] a) W. S. Kuo, C. N. Chang, Y. T. Chang, M. H. Yang, Y. H. Chien, S. J. Chen, C. S. Yeh, *Angew. Chem. Int. Ed.* **2010**, *49*, 2711; b) X. H. Huang, I. H. El-Sayed, W. Qian, M. A. El-Sayed, *J. Am. Chem. Soc.* **2006**, *128*, 2115; c) D. Pissuwan, S. M. Valenzuela, M. B. Cortie, *Biotechnol. Genet. Eng. Rev.* **2008**, *25*, 93.

[4] a) B. Li, T. Gu, T. Ming, J. Wang, P. Wang, J. Wang, J. C. Yu, *ACS nano* **2014**, *8*, 8152; b) F. Pincella, K. Isozaki, K. Miki, *Light Sci. Appl.* **2014**, *3*, e133; c) I. I. Smolyaninov, Y. J. Hung, C. C. Davis, *Science* **2007**, *315*, 1699; d) S. Tricarico, F. Bilotti, L. Vegni, *Microw. Opt. Technol. Lett.* **2009**, *51*, 2713; e) C. Wang, D. Astruc, *Chem. Soc. Rev.* **2014**, *43*, 7188.

[5] R. Gans, *Ann. Phys.* **1915**, *47*, 270.

[6] F. Wang, Y. R. Shen, *Phys. Rev. Lett.* **2006**, *97*, 206806.

[7] R. Jiang, H. Chen, L. Shao, Q. Li, J. Wang, *Adv. Mater.* **2012**, *24*, OP200.

[8] a) G. A. Sotiriou, T. Sannomiya, A. Teleki, F. Krumeich, J. Voros, S. E. Pratsinis, *Adv. Funct. Mater.* **2010**, *20*, 4250; b) C. Xue, X. Chen, S. J. Hurst, C. A. Mirkin, *Adv. Mater.* **2007**, *19*, 4071.

[9] N. Murshid, I. Gourevich, N. Coombs, V. Kitaev, *Chem. Commun.* **2013**, *49*, 11355.

[10] a) R. G. Sanedrin, D. G. Georganopoulou, S. Park, C. A. Mirkin, *Adv. Mater.* **2005**, *17*, 1027; b) M. M. Shahjamali, M. Bosman, S. Cao, X. Huang, S. Saadat, E. Martinsson, D. Aili, Y. Y. Tay, B. Liedberg, S. C. J. Loo, H. Zhang, F. Boey, C. Xue, *Adv. Funct. Mater.* **2012**, *22*, 849; c) C. Gao, Z. Lu, Y. Liu, Q. Zhang, M. Chi, Q. Cheng, Y. Yin, *Angew. Chem. Int. Ed.* **2012**, *51*, 5629.

[11] Y. Yang, J. Liu, Z. W. Fu, D. Qin, *J. Am. Chem. Soc.* **2014**, *136*, 8153.

[12] a) S. E. Skrabalak, J. Chen, Y. Sun, X. Lu, L. Au, C. M. Cobley, Y. Xia, *Acc. Chem. Res.* **2008**, *41*, 1587; b) X. Z. Gong, Y. Yang, S. M. Huang, *J. Phys. Chem. C* **2010**, *114*, 18073.

[13] I. Lee, S. W. Han, K. Kim, *Chem. Commun.* **2001**, 1782.

[14] K. Okazaki, T. Kiyama, K. Hirahara, N. Tanaka, S. Kuwabata, T. Torimoto, *Chem. Commun.* **2008**, 691.

[15] M. J. Hostetler, C. J. Zhong, B. K. H. Yen, J. Anderegg, S. M. Gross, N. D. Evans, M. Porter, R. W. Murray, *J. Am. Chem. Soc.* **1998**, *120*, 9396.

[16] Q. Zhang, J. Y. Lee, J. Yang, C. Boothroyd, J. Zhang, *Nanotechnology* **2007**, *18*, 245605.

[17] A. B. Smetana, K. J. Klabunde, C. M. Sorensen, A. A. Ponce, B. Mwale, *J. Phys. Chem. B* **2006**, *110*, 2155.

[18] C. Wang, S. Peng, R. Chan, S. Sun, *Small* **2009**, *5*, 567.

[19] a) S. Link, Z. L. Wang, M. A. El-Sayed, *J. Phys. Chem. B* **1999**, *103*, 3529; b) C. Wang, H. Yin, R. Chan, S. Peng, S. Dai, S. Sun, *Chem. Mater.* **2009**, *21*, 433; c) M. P. Mallin, C. J. Murphy, *Nano Lett.* **2002**, *2*, 1235;

[20] a) R. Rajendra, P. Bhatia, A. Justin, S. Sharma, N. Ballav, *J. Phys. Chem. C* **2015**, *119*, 5604; b) C. Gao, Y. Hu, M. Wang, M. Chi, Y. Yin, *J. Am. Chem. Soc.* **2014**, *136*, 7474.

[21] M. B. Cortie, A. M. McDonagh, *Chem. Rev.* **2011**, *111*, 3713.

[22] J. Huang, Y. Zhu, M. Lin, Q. Wang, L. Zhao, Y. Yang, K. X. Yao, Y. Han, *J. Am. Chem. Soc.* **2013**, *135*, 8552.

[23] J. Liu, L. Feng, Z. Hu, X. Hu, S. Hou, T. Wen, W. Liu, K. Zhang, X. Zhu, Y. Ji, Q. Wang, Y. Guo, X. Wu, *J. Nanosci. Nanotechnol.* **2013**, *13*, 1006.

[24] a) J. Huang, S. Vongehr, S. Tang, H. Lu, J. Shen, X. Meng, *Langmuir* **2009**, *25*, 11890; b) B. Rodríguez-González, A. Sánchez-Iglesias, M. Giersig, L. M. Liz-Marzán, *Faraday Discuss.* **2004**, *125*, 133.

[25] a) P. K. Jain, K. S. Lee, I. H. El-Sayed, M. A. El-Sayed, *J. Phys. Chem. B* **2006**, *110*, 7238; b) K. Sohn, F. Kim, K. C. Pradel, J. Wu, Y. Peng, F. Zhou, J. Huang, *ACS nano* **2009**, *3*, 2191.

[26] a) H. Kitazaki, T. Mori, J. H. Kang, T. Niidome, M. Murata, M. Hashizume, Y. Katayama, *Colloids Surf. B Biointerfaces* **2012**, *99*, 7; b) J. Zhu, Z. Yu, J. Li, J. Zhao, *Sens. Actuators, B* **2013**, *188*, 318.

[27] P. M. Gross, R. C. Taylor, *J. Am. Chem. Soc.* **1950**, *72*, 2075.

[28] C. Tyson, A. Bzowski, P. Kristof, M. Kuhn, R. Sammynaiken, T. Sham, *Phys. Rev. B* **1992**, *45*, 8924;

[29] Q. Zhang, C. M. Cobley, J. Zeng, L. P. Wen, J. Y. Chen, Y. N. Xia, *J. Phys. Chem. C* **2010**, *114*, 6396.

[30] a) S. E. Hunyadi, C. J. Murphy, *J. Mater. Chem.* **2006**, *16*, 3929; b) X. Lu, L. Au, J. McLellan, Z. Y. Li, M. Marquez, Y. Xia, *Nano Lett.* **2007**, *7*, 1764.

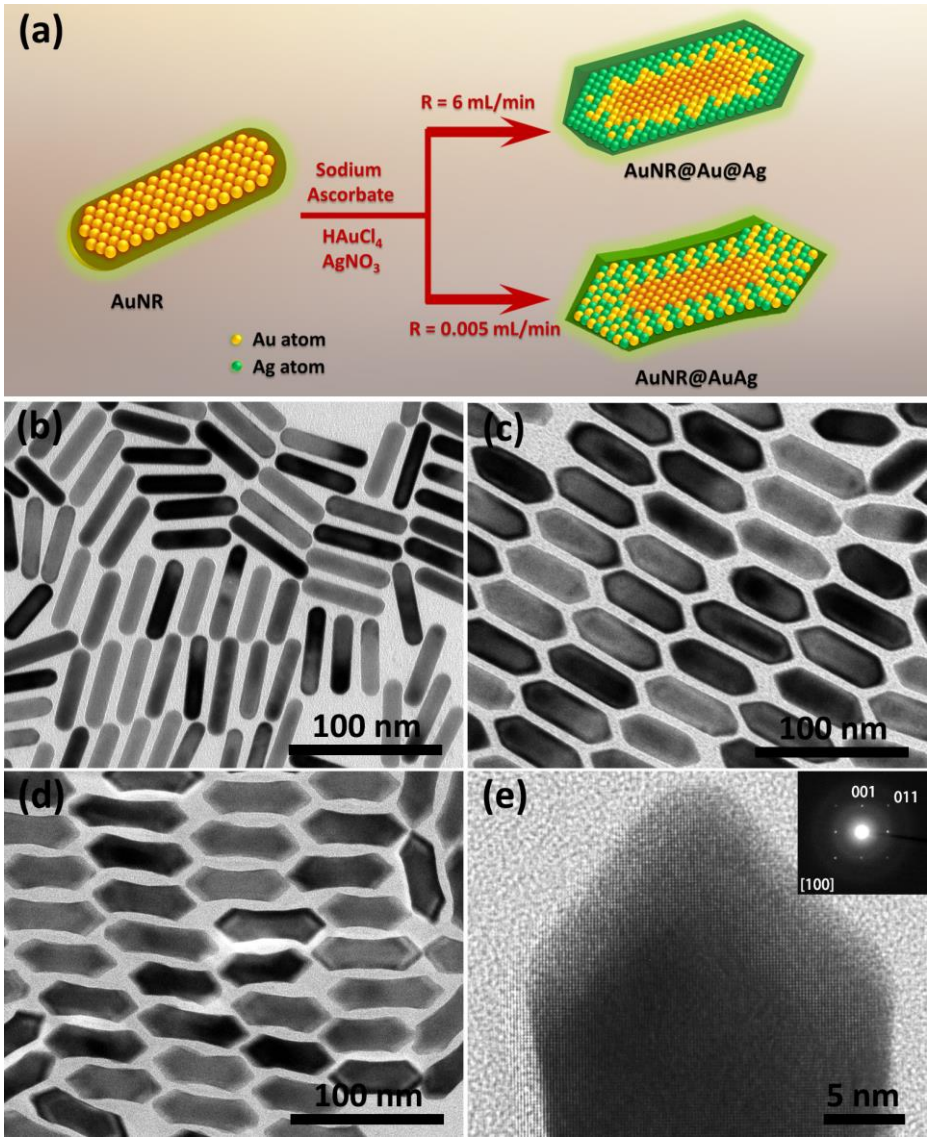

Figure 1. (a) Schematic illustration of two synthetic routes in which $AgNO_3$ and $HAuCl_4$ solutions are simultaneously infused into a AuNR seed solution at two different rates: 6 and 0.005 mL/min, and of the structures of the corresponding products, AuNR@Au@Ag and AuNR@AuAg. (b-d) TEM images of (b) the AuNR seeds, (c) AuNR@Au@Ag, and (d) AuNR@AuAg. (e) HRTEM image and ED pattern (inset) of AuNR@AuAg taken at a rod end along the [100] axis, showing the perfect epitaxial growth of the AuAg shell from the AuNR seed.

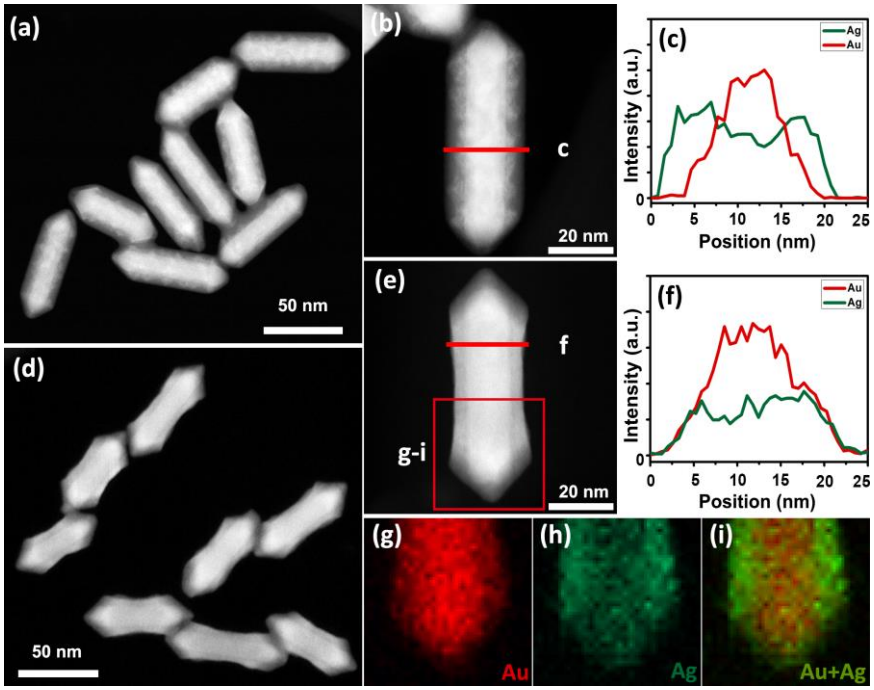

Figure 2. (a, d) Low-magnification HAADF-STEM images of (a) AuNR@Au@Ag and (d) AuNR@AuAg NRs. (b, e) High-magnification HAADF-STEM images of a single (b) AuNR@Au@Ag and (e) AuNR@AuAg NRs, and (c, f) their corresponding EDX line-scan analysis along the drawn lines. (g-i) Elemental maps of the marked area in (e) for (g) Au, (h) Ag, and (i) the superposition of Au and Ag maps, showing the uniform distribution of Au and Ag in the shell region.

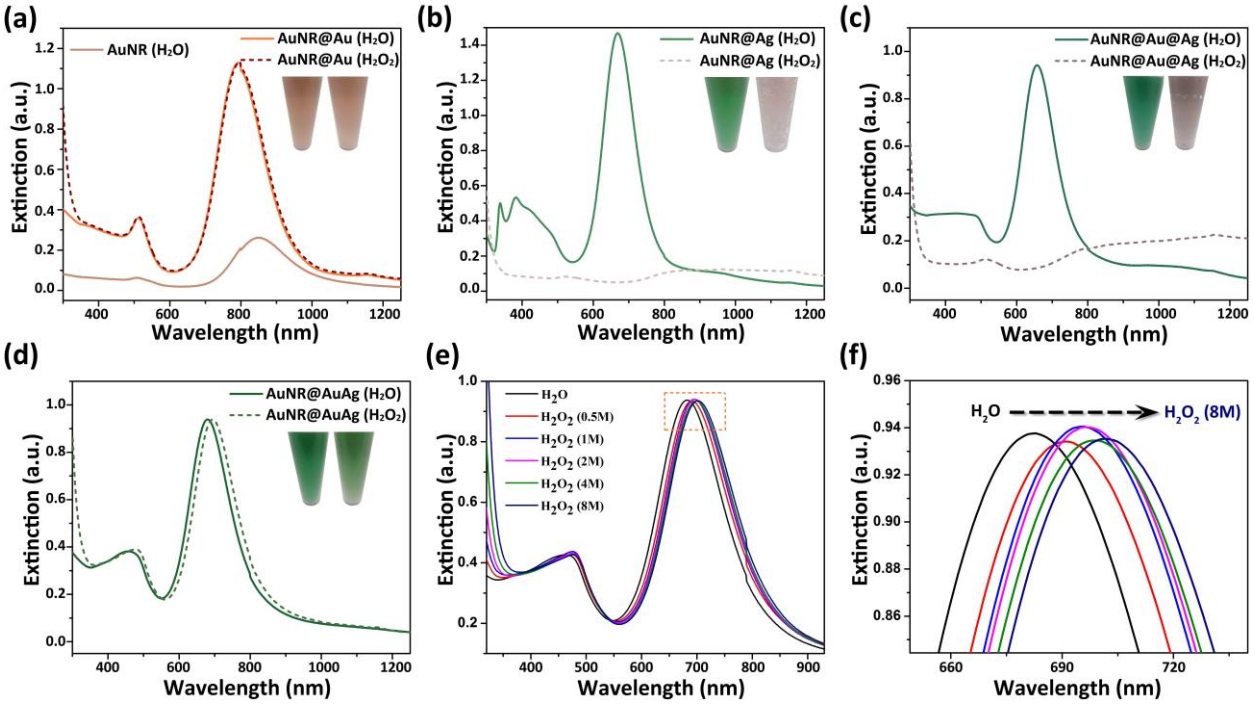

Figure 3. (a-d) UV-vis-NIR extinction spectra of (a) AuNR@Au, (b) AuNR@Ag, (c) AuNR@Au@Ag, and (d) AuNR@AuAg NRs in pure H_2O (solid line) and an aqueous solution of H_2O_2 (0.5 M) (dashed line). Insets in each panel are the corresponding visual appearance (photo pictures) of the suspension in H_2O (left) and H_2O_2 solution (right). In panel (a), the extinction spectrum of the starting AuNR seeds is also presented as a reference (the lowest curve). (e) The extinction spectra of AuNR@AuAg in different concentrations (*i.e.*, 0, 0.5, 1, 2, 4, and 8 M) of aqueous solutions of H_2O_2. (f) Enlarged extinction spectra from the marked area in pane (e). The spectra of H_2O_2-treated nanocrystals were taken after 1 h (a-d) and 24 h (e, f) of incubation in H_2O_2 solution.

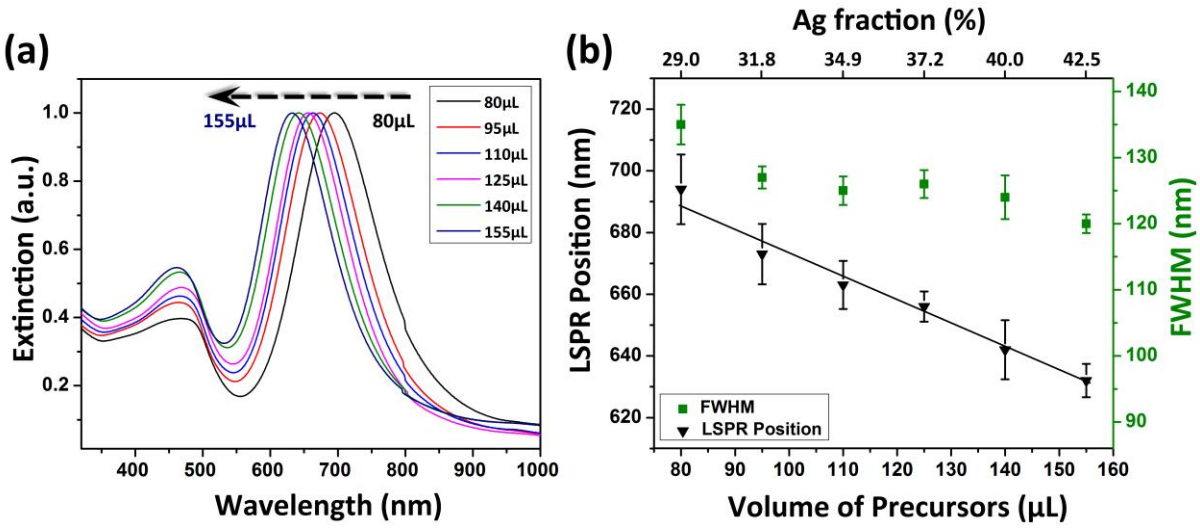

Figure 4. (a) UV-vis-NIR spectra of various AuNR@AuAg samples synthesized by using different volumes of precursors (*i.e.*, $AgNO_3$ and $HAuCl_4$). The spectra have been normalized relative to their respective maxima. (b) Dependence of the band position and FWHM of the extinction peaks of the AuNR@AuAg samples on the volume of the precursors. The corresponding Ag mole fraction in each AuNR@AuAg sample was presented in the upper x-axis. The error bars represent the standard deviation of three measurements for each sample that was synthesized in triplicate.

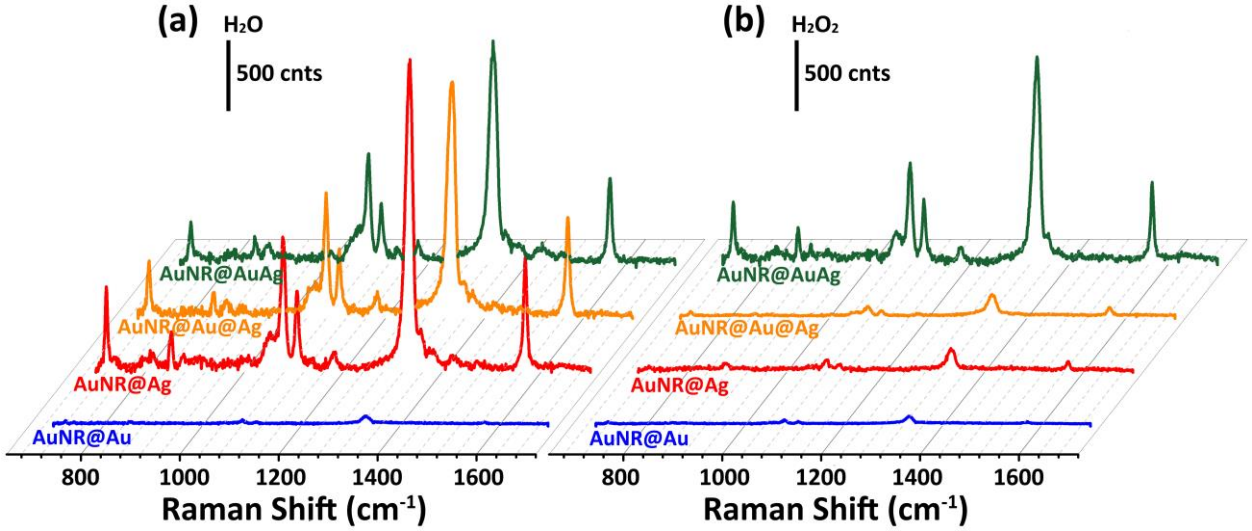

Figure 5. Colloidal SERS spectra of 4-NBT on AuNR@Au (blue), AuNR@Ag (red), AuNR@Au@Ag (orange), and AuNR@AuAg (green): (a) in H_2O and (b) after addition of H_2O_2 (0.5 M).

A facile yet effective and versatile seeded growth strategy has been developed that enables the epitaxial deposition of homogeneously alloyed AuAg shells on pre-synthesized AuNRs. The resulting AuNR@AuAg exhibits strong, stable, and tunable Surface Plasmon Resonances, implying many plasmon-mediated applications in corrosive environments.

Key words: Au nanorods, Ag stability, homogeneous AuAg alloys, tunable surface plasmon resonances, high plasmonic activities

J. Huang, Y. Zhu, C. Liu, Y. Zhao, Z. Liu, M. N. Hedhili, A. Fratalocchi and Y. Han*

Fabricating a Homogeneously Alloyed AuAg Shell on Au Nanorods to Achieve Strong, Stable, and Tunable Surface Plasmon Resonances